Numerical Simulation of the Life Cycle of a Persistent Wintertime Inversion over Salt Lake City

Linbo Wei, Zhaoxia Pu & Shigong Wang

Boundary-Layer Meteorology
An International Journal of Physical, Chemical and Biological Processes in the Atmospheric Boundary Layer

ISSN 0006-8314

Boundary-Layer Meteorol
DOI 10.1007/s10546-013-9821-2

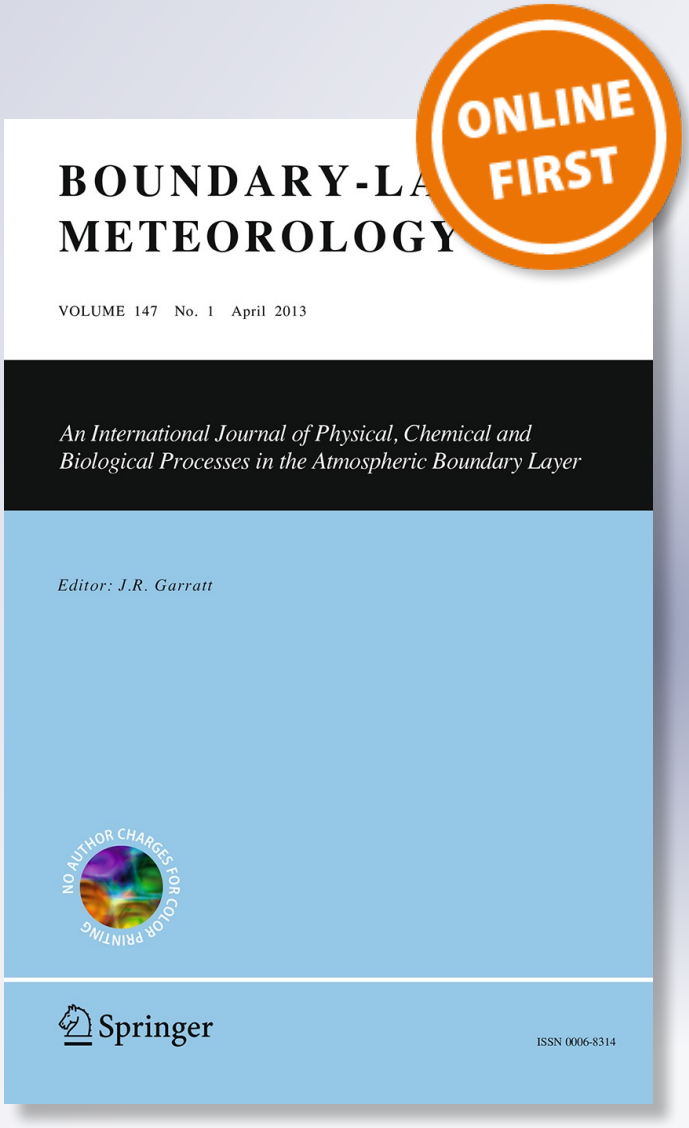

Springer

Boundary-Layer Meteorol
DOI 10.1007/s10546-013-9821-2

ARTICLE

Numerical Simulation of the Life Cycle of a Persistent Wintertime Inversion over Salt Lake City

Linbo Wei · Zhaoxia Pu · Shigong Wang

Received: 6 March 2012 / Accepted: 26 March 2013

Abstract An episode of persistent wintertime inversion over Salt Lake City, Utah and its vicinity from 1200 UTC 30 November to 0000 UTC 7 December 2010 is simulated using an advanced research version of the Weather Research and Forecasting model. The numerical simulations agree well with observed soundings in temperature, wind speed, and wind direction in the atmospheric boundary layer and above, although there are some differences near the surface due to the influence of complex terrain in the area. The characteristics of large-scale environmental conditions and their interactions with local-scale processes are analyzed to understand the factors that influence the onset and evolution of persistent inversions. It is found that the inversion formed mainly because of the interaction between the heating effect from a high-pressure ridge in the mid-troposphere and a near-surface cold pool due to the effects of radiation. During the following six to seven days, the high-pressure ridge was maintained and vertical motion very weak, allowing a persistent inversion to become established. Finally, the cold effect from a low-pressure trough in the mid-troposphere, combined with mixing due to vertical motion, led to extreme weakening of the persistent inversion.

Keywords Inversions · Mountain-valley · Numerical simulation · Salt Lake City · Weather Research and Forecasting (WRF) model

1 Introduction

In the lower troposphere, most incident shortwave radiation is absorbed by the surface and converted into sensible heat to warm the lower atmosphere, resulting in instability. The temperature typically decreases with altitude in the planetary boundary layer. Sometimes, how-

L. Wei · S. Wang
College of Atmospheric Sciences, Lanzhou University, Lanzhou, Gansu, China

L. Wei · Z. Pu (✉)
Department of Atmospheric Sciences, University of Utah, 135 South 1460 East, Rm. 819, Salt Lake City, UT 84112, USA
e-mail: Zhaoxia.Pu@utah.edu

Published online: 10 April 2013

ever, the temperature increases or becomes nearly neutral with altitude, leading to buoyancy-induced vertical motion being suppressed, with positive stability of the atmosphere. This deviation from the usual temperature pattern is the so-called inversion.

Inversions can affect human lives and health because the stable air traps air pollutants near the surface and allows for an unacceptable and harmful concentration (Holzworth 1962, 1967; Reddy et al. 1995; Reeves and Stensrud 2009). They are also related to fogs and extreme temperature minima that affect human activities and plant growth, especially in wintertime.

Inversions commonly tend to form under conditions of complex terrain, weak surface winds, and clear night skies. Complex terrain, such as valleys and basins, not only produces cold downslope flows (Colette et al. 2003) but also blocks cold air inside the valleys or basins (Wolyn and McKee 1989). Weak surface winds prohibit thermal advection. Clear skies enhance heat loss and cooling at the surface, especially during the long winter nights in mid-latitudes, where nighttime surface cooling continues for a longer period. In light of these factors, it is not surprising that inversions are more widespread over the mountainous areas of the western USA than elsewhere in the country and more frequent during the winter than in other seasons.

There are usually two categories of inversion in the mountainous areas of the western USA, defined by their duration: diurnal inversions and persistent inversions. A diurnal inversion can occur in both flat terrain, as shown in Colette et al. (2003), and in valleys or basins, according to Müller and Whiteman (1987) and Whiteman and Pospichal (2004). It can occur at night under conditions of weak surface winds and clear skies in the upper troposphere, and it dissipates after sunrise. A persistent inversion, or long-term inversion, however, is usually formed in valleys or basins in winter due to elevated terrain that can attain cold and stable air stagnant for a long period (Wolyn and McKee 1989). Unlike a diurnal inversion, a persistent inversion can survive under solar radiation and last for several days. Relatively stable atmospheric conditions and suitable synoptic processes, such as a large-scale ridge in the upper troposphere, are necessary for its formation and continuation (Wolyn and McKee 1989; Whiteman et al. 1999).

There have been many climatological and numerical studies on persistent inversions. Based on the analysis of a large sample of soundings, Wolyn and McKee (1989) concluded that deep stable layers lasting three days or more occur over Salt Lake City at least once every two years. In their study of a persistent wintertime inversion in Colorado, Whiteman et al. (1999) analyzed radiosonde data and indicated that the buildup of such inversions takes place as warm air advection occurs above a basin with the approach of a high-pressure ridge in the middle troposphere, while they are broken up with cold air advection above the basin as a trough approaches. Gillies et al. (2010a,b) pointed out that the development of persistent inversions over Salt Lake Valley closely follows either 6-day or 30-day patterns, which are driven by distinct dynamics as reflected in their different dimensions and propagation properties. They also proposed a regression method coupled with the Climate Forecast System (CFS) fields to predict persistent inversion events with lead times of up to 4 weeks. Many other studies, such as Wendisch and Mertes (1995), Colette et al. (2003), and Zoumakis and Efstathiou (2006a,b), have paid great attention to forecasting and the mechanisms behind the initiation or dispersal phases of inversions.

Salt Lake City is situated in the Salt Lake Basin and surrounded by mountains except on the western side, where the Great Salt Lake (GSL) is located (Fig. 1). Due to the characteristics of the surrounding terrain, Salt Lake City experiences inversions and poor air quality almost every winter. Inversions in Salt Lake Valley have been the subject of previous studies by Wolyn and McKee (1989), Whiteman et al. (1999), and Gillies et al. (2010a,b). However, *modelling work that simulates a relatively complete episode of the formation and continuation*

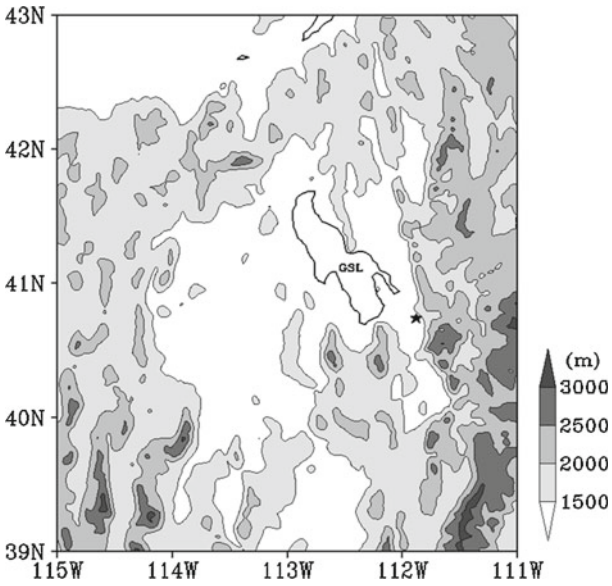

Fig. 1 Location and topography of Salt Lake City and its vicinity: GSL denotes Great Salt Lake. The *star* represents the location of Salt Lake City

of a persistent inversion in Salt Lake City is generally lacking. Therefore, in this study, the life cycle of a persistent wintertime inversion over Salt Lake City is simulated with the Weather Research and Forecasting (WRF) model. Our purpose is to understand the mechanisms of large-scale and mesoscale environmental conditions that contribute to the formation, maintenance, and weakening of inversions. The ability of the WRF model to simulate wintertime inversions is also evaluated by comparing the inversion characteristics generated by the model simulation with the sounding observations.

The paper is organized as follows: Sect. 2 introduces the persistent inversion case, while Sect. 3 describes the numerical model and the experiment design. Section 4 discusses the simulation results, including an evaluation of the ability of the WRF model to simulate wintertime inversions and an analysis of synoptic processes, local thermodynamics, and kinetic processes during the formation and continuation phases of the persistent inversion. Section 5 examines the sensitivity of numerical simulation to model vertical resolution, and Sect. 6 provides a summary and conclusions.

2 Description of a Persistent Inversion over Salt Lake City

2.1 The Definition of a Persistent Inversion

Wintertime inversions over the mountainous areas in the western USA can be categorized as capping inversions or surface-based inversions, depending on whether the base of the inversion is in contact with the surface. A capping inversion refers to an inversion layer whose base is elevated above the surface. A surface-based inversion is a stable layer extending from the surface to a certain altitude, which is called the inversion top. As described in the previous section, inversions can also be classified as diurnal or persistent, depending on their duration. A persistent inversion, which may be a capping inversion, a surface-based inversion, or both, can survive under daytime solar radiation and last for several days.

Following Wolyn and McKee (1989), a lapse rate ($\partial T/\partial z$) of 2.5 K km^{-1} is used as a threshold to define an inversion, where T is the air temperature as the threshold was derived from the sounding profiles. If the lapse rate $\leqslant$2.5 K km^{-1} in the lower troposphere, the layer is defined as an inversion. The inversion top is defined as a height or pressure level at which the lapse rate changes from $\leq$2.5 to $>$2.5 K km^{-1}. In addition to the lapse rate, wind speed and/or direction are also used to define an inversion top. For instance, Reeves and Stensrud (2009) defined an inversion top as a level under which the wind speed $<$5 m s^{-1}. Gillies et al. (2010a,b) defined an inversion top as a wind- direction change exceeding 60° or a wind-speed change of more than 10 m s^{-1}. Considering the downward transfer of warmer air during the formation of the inversion, the wind vector is not used as a criterion to define the inversion top in this study.

Inversions are commonly characterized by their depth and strength (Whiteman et al. 1999; Liu and Key 2003). Depth refers to the height difference between the inversion top and base, namely, inversion depth $D = H_{\text{top}} - H_{\text{base}}$, where H_{top} and H_{base} refer to the height of the inversion top and base, respectively. Strength is defined as the temperature difference between the inversion top and base divided by the inversion depth: $S = (T_{\text{top}} - T_{\text{base}})/(H_{\text{top}} - H_{\text{base}})$, where T_{top} and T_{base} refer to the air temperature of the inversion top and base, respectively. In this study, besides depth and strength, we also use pressure at the inversion top to describe the life cycle of the persistent inversion. Since the surface pressure changes significantly with time (see Fig. 4), the pressure at the inversion top can roughly represent the height from the surface to the inversion top.

2.2 Data

As shown in Fig. 1, Salt Lake City, with an average elevation of 1,320 m above mean sea level, is situated in the Salt Lake Valley, and surrounded by mountains from the north to the south west and by the Great Salt Lake to the west. The highest surrounding mountain range is the Wasatch Range to the east, which reaches a height of about 3.45 km. The second-highest mountain range is the Oquirrh Mountains, with a maximum height of about 3.24 km. In the valley, the KSLC meteorological sounding station is located at the Salt Lake City International Airport, west of the city, at an elevation of 1.29 km. This station provides complete, quality sounding data for the valley that is important in determining the persistent inversion episode, evaluating the WRF numerical simulation, and helping analyze the inversion mechanisms. The temporal interval of the soundings is 12 h.

Besides the KSLC soundings, hourly surface mesonet observations (Horel et al. 2002; also see http://mesowest.utah.edu) are adopted to verify the model performance in terms of the near-surface variables. In addition, analysis data from the National Centres for Environmental Prediction (NCEP)'s North American Mesoscale (NAM) model are utilized to provide the synoptic background for the analysis of the inversion process. The temporal interval and horizontal resolution of the NAM data are 6 hand 12 km, respectively.

Coordinated universal time (UTC) is used throughout this paper; the local time (LT) of Salt Lake City in winter is 7 h behind UTC. "Daytime" is used to represent the period from 1200 UTC (0500 LT) to 0000 UTC (1700 LT), and "nighttime" is used to refer to the period from 0000 UTC (1700 LT) to 1200 UTC (0500 LT).

2.3 A Brief Overview of the Persistent Inversion Case

Soundings from KSLC station are used to determine the observed properties of the persistent inversion in Salt Lake City. The position of the inversion top is determined by analyzing

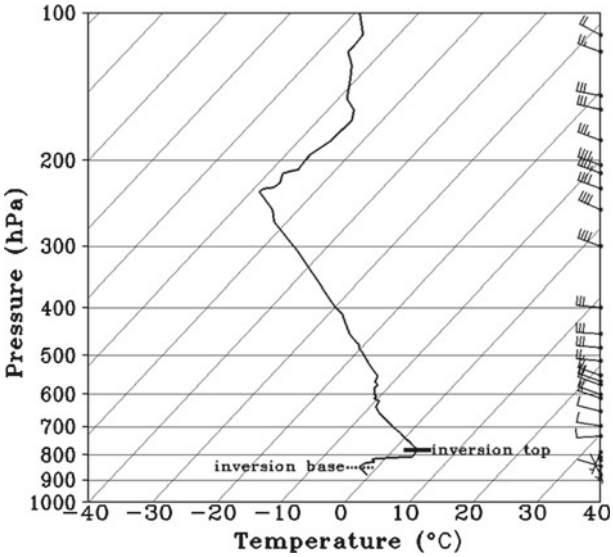

Fig. 2 A sample Skew-T from soundings at the KSLC station at 0000 UTC 2 December 2010. The *solid* and *dashed lines* represent the inversion top and base, respectively. Each short (or long) wind barb represents $5\,\mathrm{m\,s^{-1}}$ (or $10\,\mathrm{m\ s^{-1}}$) and each pennant represents $50\,\mathrm{m\ s^{-1}}$. Wind barbs have the same implication in the other figures

Skew-T plots. A sample Skew-T plot at 0000 UTC 2 December is shown in Fig. 2a, with the inversion top and base fixed at about the 770-hPa and 850-hPa pressure levels, respectively. The inversion type, top height, base height, and depth from soundings between 1200 UTC 30 November and 0000 UTC 7 December are listed in Table 1. It is apparent that a complex inversion first formed at 1200 UTC 30 November, including a surface-based inversion near the surface and a capping inversion above. Between 1200 UTC 30 November and 1200 UTC 3 December, the inversion top decreased from about 600 hPa to 820 hPa, then fluctuated around 800 hPa. From 1200 UTC 6 December to 0000 UTC 7 December, the inversion top decreased to near the surface level. After 0000 UTC 7 December, the inversion top increased significantly (not shown), corresponding to another inversion episode. Hence, the period from 1200 UTC 30 November to 0000 UTC 7 December is chosen as a complete persistent inversion episode in this study.

3 Numerical Model and Experimental Design

The numerical model employed in this study is the Advanced Research version 3.1.1 of the WRF model (ARW). The ARW model is compressible and non-hydrostatic, with a terrain-following hydrostatic pressure coordinate and the Arakawa C-grid. Runge-Kutta second- and third-order time integration schemes, second- and sixth-order advection schemes in both the horizontal and vertical directions, and a time-split small step for acoustic and gravity-wave models, are used. A detailed description of the ARW model can be found in Skamarock et al. (2008).

We use high-resolution numerical simulations to simulate low-level inversions. A two-way interactive, three-level nested domain technique is used in the experiment. The spatial range

Table 1 Type, top height, base height, and strength of the inversion from soundings at KSLC from 1200 UTC 30 November to 0000 UTC 7 December 2010 ("s" and "c" represent surface-based inversion and capping inversion, respectively; "com" represents a complex inversion that includes both "s" and "c")

Time	Inversion type	Top height (km)	Base height (km)	Depth (km)	Strength (K km^{-1})
1200 UTC 30 Nov	com	2.74	0.00	2.74	−0.07
0000 UTC 1 Dec	c	1.94	0.68	1.26	1.04
1200 UTC 1 Dec	s	1.59	0.00	1.59	−0.35
0000 UTC 2 Dec	c	1.05	0.26	0.80	6.94
1200 UTC 2 Dec	s	0.73	0.00	0.73	12.87
0000 UTC 3 Dec	c	0.70	0.21	0.49	12.53
1200 UTC 3 Dec	s	0.48	0.00	0.48	17.87
0000 UTC 4 Dec	s	1.24	0.00	1.24	−1.16
1200 UTC 4 Dec	s	1.25	0.00	1.25	2.88
0000 UTC 5 Dec	c	0.74	0.43	0.30	14.28
1200 UTC 5 Dec	s	0.84	0.00	0.84	1.19
0000 UTC 6 Dec	c	1.16	0.26	0.90	3.10
1200 UTC 6 Dec	s	0.23	0.00	0.23	30.64
0000 UTC 7 Dec	s	0.35	0.00	0.35	−1.14

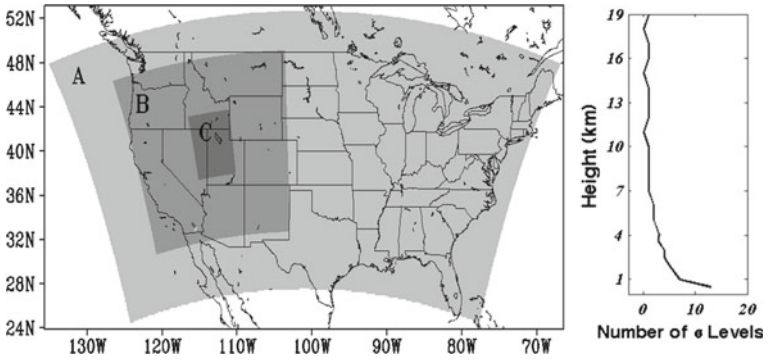

Fig. 3 Locations of the model domains for the WRF model numerical simulation (*left panel*). Domain A is at 12-km resolution. Domains B and C are the nested grids at 4-km and 1.33-km resolutions, respectively. The *right panel* shows the variation in the number of vertical model sigma levels with height

of the three domains is shown in Fig. 3a; the coarse domain (Domain A) covers most of the United States, with the centre at (40°N, 101°E) and a horizontal resolution of 12 km, which is the same horizontal resolution as the NCEP NAM analysis. The number of grid points in the coarse domain is 400 × 230. The second domain (Domain B) covers the mountainous areas over the western USA, where persistent wintertime inversions mainly occur. The horizontal resolution of this domain is 4 km, and the number of grid points is 421 × 442. The third nested domain (the innermost, Domain C) covers most of the state of Utah, including the Salt Lake Valley and the surrounding mountains, which may have topographic influence on persistent inversions in Salt Lake City. The horizontal resolution of the third domain is about 1.33 km, and the number of grid points is 319 × 463.

In order to simulate the life cycle of the aforementioned persistent inversion, the simulation period covers 10 days, from 0000 UTC 29 November to 1200 UTC 8 December 2010. For the numerical simulation, initial and boundary conditions are derived from the NCEP NAM model analysis by the WRF pre-process. Sixty σ levels (see Fig. 3b) are set vertically for the WRF model, with 20 σ levels below 1 km, and 16.3 m as the lowest model level to obtain relatively high-resolution data on the boundary-layer structure. The following model physics options are used: the WRF single-moment six-class cloud microphysics by Hong et al. (2004), the RRTM longwave radiation scheme by Mlawer et al. (1997), the Dudhia shortwave radiation scheme by Dudhia (1989), the Noah land-surface model as described by Chen and Dudhia (2001), and the Mellor–Yamada–Janjic planetary boundary-layer (PBL) scheme from Janjic (2002). The Kain–Fritsch cumulus parametrization referred to by Kain and Fritsch (1990) is applied for Domain A only.

4 Simulation Results

4.1 Comparison Between the Simulation and Soundings

In order to validate the persistent inversion simulated by the WRF model, the simulation results are compared with the soundings at the KSLC station. Figure 4 shows a time series of temperature, wind, and the inversion top from the soundings and the simulation along with the surface pressure from the soundings (the surface pressure from the simulation is almost coincident with that from the soundings, so it is not shown). It is clear that the simulated temperature, wind speed, and wind direction mostly agree with the sounding observations above 800 hPa, although there are some discrepancies at lower levels due to the influence

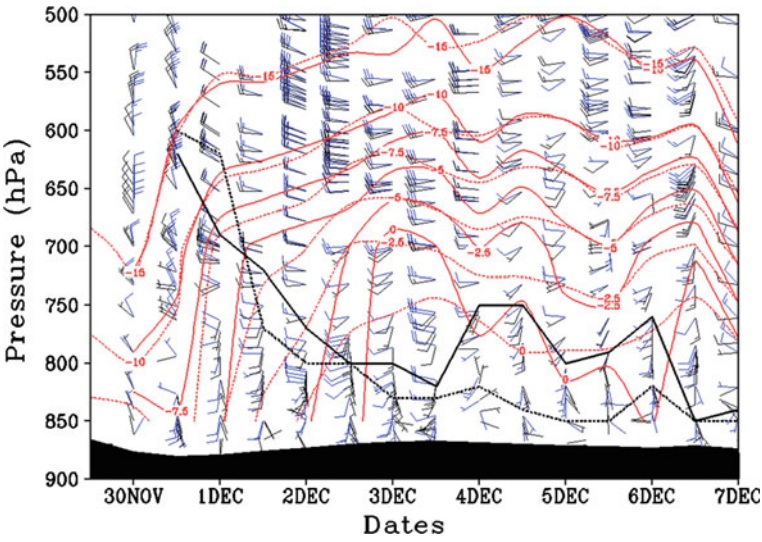

Fig. 4 Comparison of wind speed ($m\,s^{-1}$), temperature (°C), and the inversion top (hPa) from soundings and the simulation at KSLC during 0000 UTC 30 November to 0000 UTC 7 December 2010. *Black* and *blue wind bars*, *solid* and *dashed red contours*, and *solid* and *dashed lines* represent wind, temperature, and the inversion top from soundings and the simulation, respectively. The *shading* at the bottom of the plot represents the surface pressure

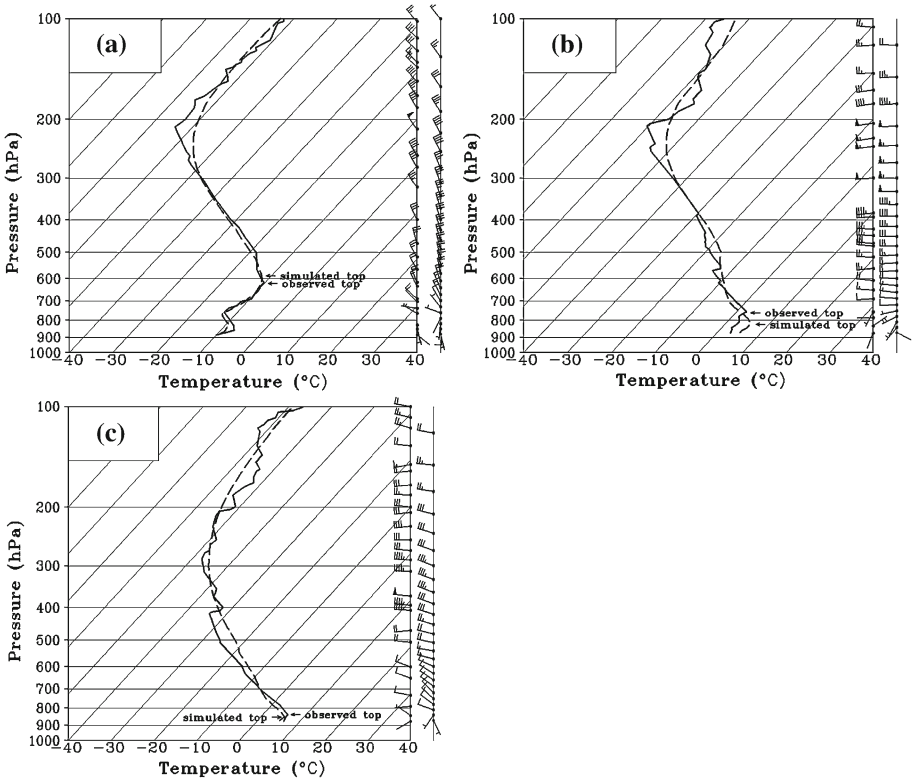

Fig. 5 Comparison of temperature (°C) and wind (m s^{-1}) between soundings and the simulation at KSLC at **a** 1200 UTC 30 November, **b** 0000 UTC 4 December, and **c** 0000 UTC 7 December 2010. *Solid* and *dashed contours* and wind barbs in the *left* and *right columns* represent temperature and wind from soundings and the simulation, respectively. "Simulated top" and "observed top" mean the inversion top derived from the simulation and soundings, respectively

of terrain. Differences in wind direction are clearly evident, although the wind speed from the simulation and the sounding observations is similar most of the time. The inversion tops from the simulation are below those from the soundings except during the beginning of the inversion.

Figure 5 further compares the sounding profiles of temperature and wind at KSLC at 1200 UTC 30 November, 0000 UTC 4 December, and 0000 UTC 7 December, which represent the formation, continuation, and dissipation of the persistent inversion, respectively. It indicates that although the simulated temperature and wind profiles differ somewhat from the sounding observations near the surface, their variations with height are basically consistent with the sounding observations.

The depth, strength, and pressure of the inversion top from the simulation are listed in Table 2. Comparing Tables 1 and 2, it is apparent that the WRF model has difficulty in simulating inversion types. This may be attributed to model errors near the surface. It is also found that large (small) depths correspond to weakness (strength) in both the soundings and the simulation most of the time (Fig. 6). The depths from the soundings and the simulation coincide most of the time, except for the periods of 0000 UTC to 1200 UTC 1 December, 0000 UTC to 1200 UTC 4 December, and 0000 UTC to 1200 UTC 5 December. In addition,

Table 2 Same as Table 1, except showing the simulated results

Simulation time	Inversion type	Top height (km)	Base height[a] (km)	Depth (km)	Strength (K km^{-1})
1200 UTC 30 Nov	com	2.96	0.00	2.96	0.78
0000 UTC 1 Dec	s	2.75	0.00	2.75	−0.50
1200 UTC 1 Dec	s	1.05	0.00	1.05	6.26
0000 UTC 2 Dec	c	0.73	0.16	0.58	4.74
1200 UTC 2 Dec	s	0.72	0.00	0.72	4.05
0000 UTC 3 Dec	s	0.40	0.00	0.40	13.99
1200 UTC 3 Dec	s	0.39	0.00	0.39	11.50
0000 UTC 4 Dec	s	0.51	0.00	0.51	5.11
1200 UTC 4 Dec	s	0.32	0.00	0.32	10.29
0000 UTC 5 Dec	s	0.23	0.00	0.23	6.04
1200 UTC 5 Dec	s	0.24	0.00	0.24	15.36
0000 UTC 6 Dec	s	0.55	0.00	0.55	1.65
1200 UTC 6 Dec	s	0.24	0.00	0.24	13.94
0000 UTC 7 Dec	s	0.26	0.00	0.26	12.18

[a] Due to the use of air temperature at 2-m height to define the inversion base, the base heights here are nearly zero, as in almost all cases the bases of inversions are found to be at 2-m height. This fact, however, reflects the mesoscale model's inability in resolving the near-surface atmospheric structures

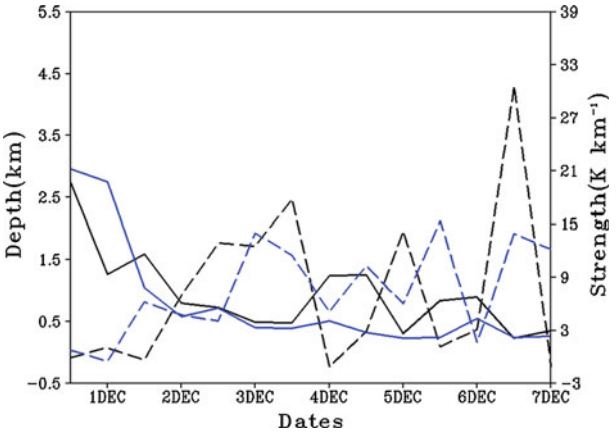

Fig. 6 Depth and strength of the inversion from soundings and the simulation at KSLC from 1200 UTC 30 November to 0000 UTC 7 December 2010. The *solid* and *dashed black lines* represent the depth and strength of the inversion from soundings, respectively, and the *solid* and *dashed blue lines* represent those from the simulation

the strength from the simulation differs considerably from that of the sounding observations, mainly reflecting the discrepancies between the near-surface conditions of the soundings and the simulation.

Overall, the numerical simulation successfully simulates the evolution of the persistent inversion. The major discrepancies between the soundings and the simulation are caused mainly by the simulation errors near the surface. Since the simulated key atmospheric conditions, including temperature and wind, are consistent with the observations above 800 hPa

(immediately above the near-surface layer over the mountain-valley area), it is reasonable to use the numerical simulation results to analyze the large-scale and mesoscale environmental conditions associated with the persistent inversion.

4.2 Large-Scale Synoptic Processes

4.2.1 Cold Pool

The near-surface cold pool and horizontal advection in the lower atmosphere are also examined. Figure 7 shows near-surface temperature and wind fields from the simulation and surface mesonet observations. Although discrepancies exist between the simulation and mesonet observations in terms of details in the surface wind and temperature, overall patterns of temperature distribution and advection correspond well. The strengthening and extension of the cold pool are also clearly seen in the simulation.

During the formation of the inversion (Fig. 7a), air in the south of the Salt Lake Valley was colder than the air over Salt Lake City. There was a surface cold air pool to the south and southwest of Salt Lake City. The low-level flow was from the south to Salt Lake City, presenting cold-air horizontal advection and a supply of cold air to cool the lower atmosphere and thus enhance the formation of the inversion. However, from 1200 UTC 1 December to 0000 UTC 3 December, the air temperature in the south of Salt Lake Valley was higher than that over Salt Lake City. The warm air was transferred from the south to Salt Lake City through horizontal advection and so increase the temperature. Around 1200 UTC 3 December, with the passage of a cold front, wind speed was quite high and temperatures decreased. A near-surface cold pool was formed near Salt Lake City and its southern and western vicinities (Fig. 7b). From 1200 UTC 4 December to 0000 UTC 6 December, the horizontal advection was very weak (Fig. 7c). The relatively calm atmosphere provided a favorable condition for maintaining the inversion during this period. From 1200 UTC 6 December to 0000 UTC 7 December, the warm-air advection (Fig. 7d) was strengthened with the increase of wind speeds, resulting in a significant weakening of the inversion.

4.2.2 High-Pressure Systems in the Lower Atmosphere

Persistent wintertime inversions, as opposed to nocturnal inversions, can survive under solar radiation and remain for several days. Hence, large-scale synoptic processes play a very important role in the life cycle of persistent inversions. Around 1200 UTC 30 November, when the inversion formed, a surface high-pressure system dominated the Salt Lake Valley area (not shown), and this high-pressure system persisted until 0000 UTC 1 December, although its central pressure decreased. Except for a short period around 1200 UTC 3 December, when a cold front passed from the north, Salt Lake City was controlled by high-pressure systems until early 6 December. From 1200 UTC 6 December to 0000 UTC 7 December, a low-pressure system (not shown) from the ocean passed over Salt Lake City and the inversion was greatly weakened.

4.2.3 500 hPa High-Pressure Ridge

Corresponding to the pressure systems at lower levels, synoptic processes at the 500-hPa level also played an important role during the persistent inversion. As shown in Fig. 8a, during the formation of the inversion, Salt Lake City was under a deep high-pressure ridge, coinciding with high-pressure systems at the surface. The high-pressure ridge supplied relatively warm

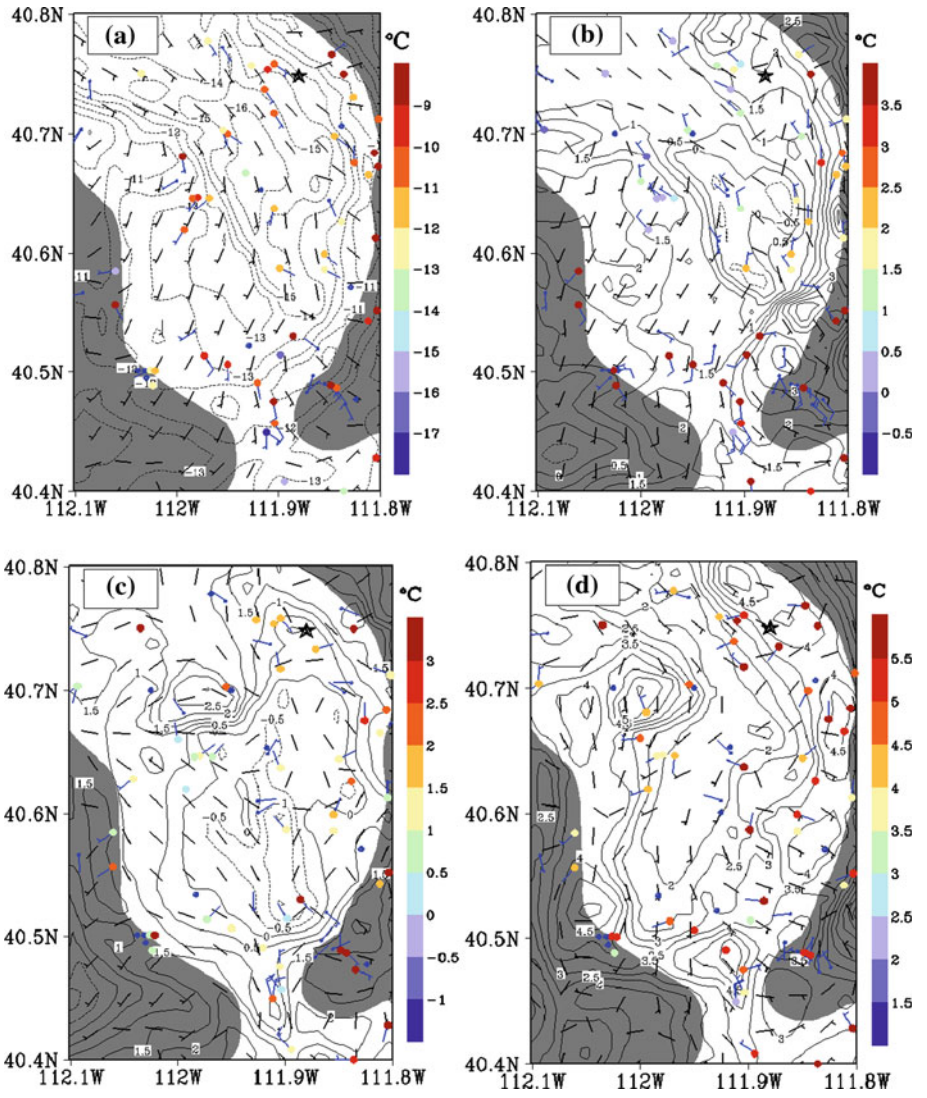

Fig. 7 Near-surface temperature (*contour*) and winds (*black barbs*) from simulations and temperature (*colour dots*) and winds (*blue barbs*) from surface Mesonet observations at **a** 1200 UTC 30, November, **b** 0000 UTC 03 December, **c** 0000 UTC 06 December and **d** 0000 UTC 7 December 2010. *Shaded contours* denote the mountains around the Salt Lake City area. The *star* indicates the location of Salt Lake City

air to heat the mid-troposphere, providing a favourable condition for the formation of the inversion. After that, the ridge persisted over the Salt Lake City area during the continuation phase of the inversion (Fig. 8b) and ensured that the atmosphere aloft was warmer than that at lower levels during both daytime and nighttime. Finally, around 0000 UTC 7 December, a low-pressure trough at 500 hPa passed over Salt Lake City (Fig. 8c). With the subsequent cold-air advection, the inverted temperature structure was destroyed, resulting in a marked weakening of the inversion. Meanwhile, a weak low-pressure system appeared at the surface around Salt Lake City. Shortly after that, another high-pressure ridge passed over Salt Lake

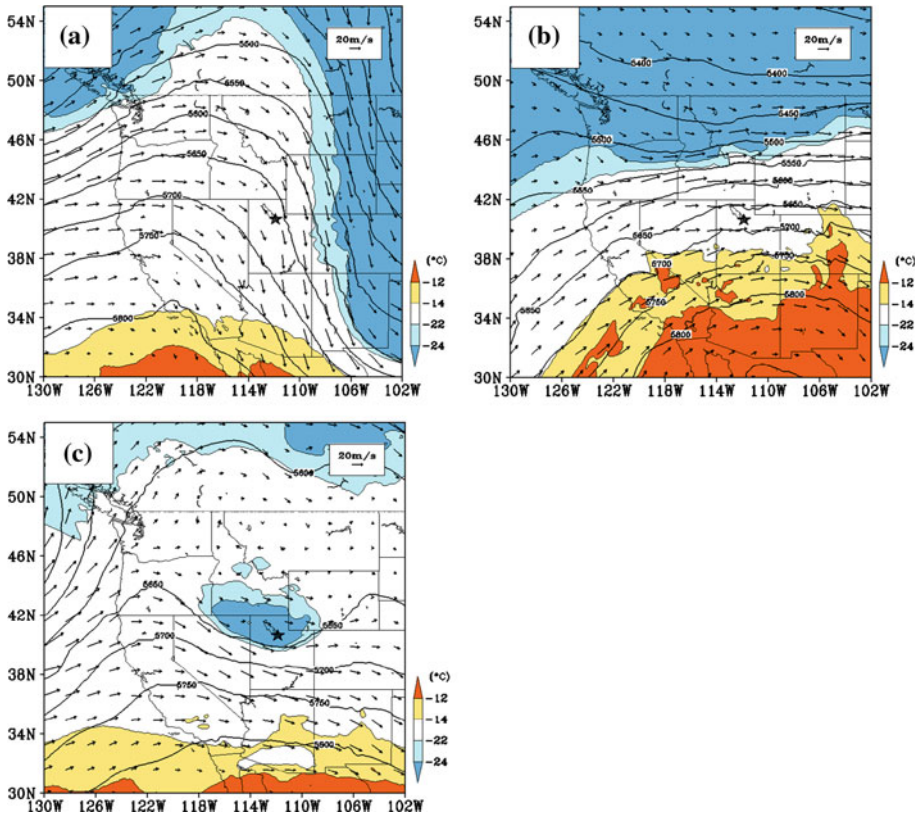

Fig. 8 Geopotential height (*contour*), temperature (*shading*), and wind vector (*arrows*) at 500 hPa. **a** 1200 UTC 30 November, **b** 1200 UTC 3 December, and **c** 0000 UTC 7 December 2010. The *star* represents the location of Salt Lake City

City, corresponding to another inversion episode, indicating the end of the persistent inversion episode studied herein. The importance of a successive high-pressure ridge and low-pressure trough during a persistent inversion has also been indicated by Wolyn and McKee (1989) and Whiteman et al. (1999).

4.3 Circulations

4.3.1 Vertical Circulation

In order to analyze the influence of vertical motion on the persistent inversion, the relationship between the vertical velocity and the inversion top at the KSLC station from 0000 UTC 29 November to 0000 UTC 7 December is investigated. As Fig. 9 indicates, around the early phase of the inversion, the vertical motion at low levels was very weak, which favoured the formation of the inversion. Around 1200 UTC 3 December, there was apparent downward vertical motion, resulting in the descent of potentially warmer air. Meanwhile, the height of the observed inversion top was reduced, and the simulated inversion top remained at a lower level. After that, the air was relatively calm, and the top of the inversion was lifted. Around 1200 UTC 6 December, downward vertical motion above 500 hPa brought potentially warm

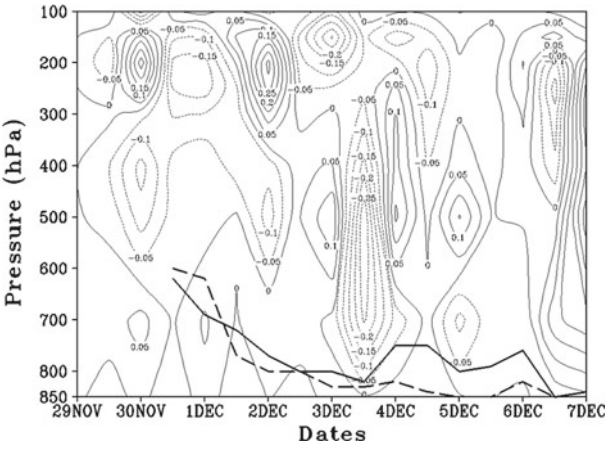

Fig. 9 Vertical velocity (*contours*) from the simulation, and the inversion top from soundings (*solid bold line*) and the simulation (*dashed bold line*) from 0000 UTC 29 November to 0000 UTC 7 December

air downward, and upward motion below 500 hPa brought relatively cold air upward. The subsequent mixing resulted in the descent of the inversion top.

During the persistent inversion, the surface of the Wasatch Range to the east of Salt Lake City was much colder than the atmosphere. This air over the colder mountains formed cold downslope flows thus providing cold air supplies for the formation of the inversion. The wind direction east of Salt Lake City was eastward (see Fig. 7c). Meanwhile, the flow above the Wasatch Range was weak (not shown). Both were beneficial to the formation of the inversion. When the cold front passed over Salt Lake City around 1200 UTC 3 December and a low-pressure system passed through Salt Lake City around 0000 UTC 7 December, the wind speed above the Wasatch Range was much greater than at other times during the persistent inversion, corresponding to the lower inversion top.

4.3.2 Horizontal Advection

In their study on the evolution of a wintertime inversion in the Colorado Plateau Basin, Whiteman et al. (1999) pointed out that the build-up of wintertime inversions takes place over one or more days as warm air advection occurs above a basin, and the break-up of an inversion occurs with cold air advection above the basin. In the current case, significant warm-air and cold-air advections were found in the formation (Fig. 8a) and weakening (Fig. 8c) phases at 500 hPa, respectively. Warm advection is the main cause of upper-air warming, which is important for the formation of an inverted temperature structure.

The horizontal advection at 850 hPa is also examined using the simulation results (not shown). During the formation of the inversion, the wind direction was from the south of the Salt Lake Valley and brought relatively cold air to Salt Lake City. After that, the air temperature above the southern Salt Lake Valley was higher than that over Salt Lake City at 850 hPa. The relatively warm air was the main reason for the temperature increase in Salt Lake City, which is also seen in the surface mesonet observations (not shown). From 1200 UTC 4 December to 0000 UTC 6 December, the horizontal advection at 850 hPa was very weak. From 1200 UTC 6 December to 0000 UTC 7 December, the warm advection was strengthened with the increasing wind speed, corresponding to the pronounced weakening of the inversion.

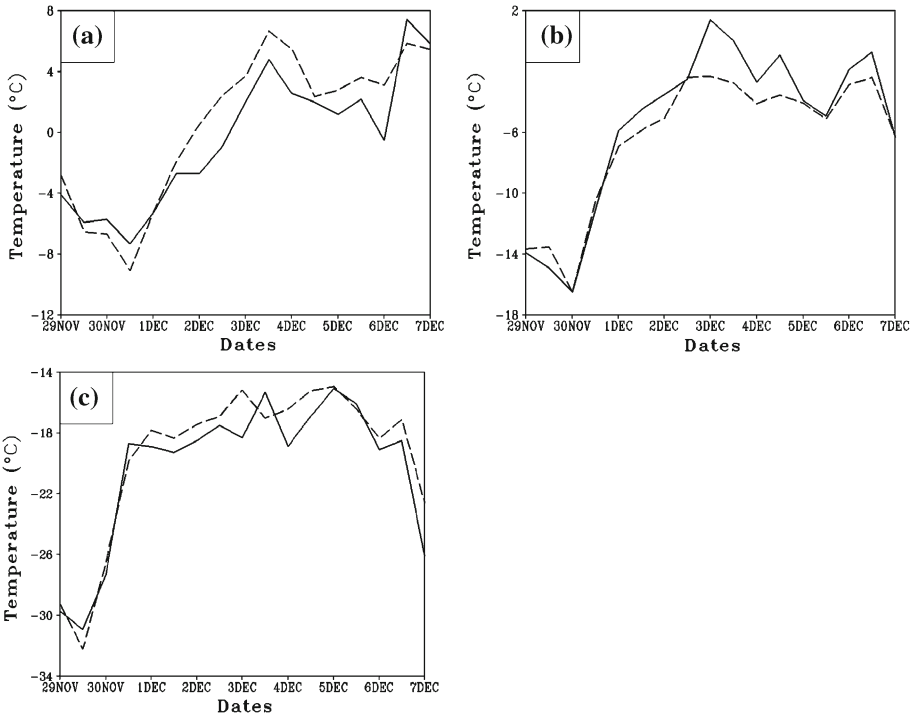

Fig. 10 Temperature at **a** 850 hPa, **b** 700 hPa, and **c** 500 hPa from soundings (*solid*) and the simulation (*dashed*)

4.4 Physical Processes

4.4.1 Temperature Variation

An inversion is a stable layer in which the temperature increases with height. Inverted temperature structure is the primary characteristic of an inversion. Time series of temperatures from KSLC soundings at 850 hPa, 700 hPa, and 500 hPa from 0000 UTC 29 November to 0000 UTC 7 December are illustrated in Fig. 11a. For convenience, these are referred to as low-, mid-, and high-level temperature, respectively, in the rest of this section. Figure 10a–c shows temperatures from the soundings and the simulation at 850 hPa, 700 hPa, and 500 hPa, respectively. The variation of the simulated temperature is similar to that of the soundings at the three pressure levels.

From the sounding temperatures, it is clear that before 1200 UTC 29 November, the temperature between 850 hPa and 500 hPa decreased, indicating that the cold pool was strengthened. Then, with the transfer of relatively warm air to lower levels, the temperature increased from higher to lower levels sequentially. From 1200 UTC 29 November to 0000 UTC 30 November, the temperature at 500 hPa increased, while the temperature continued to decrease at 700 hPa and 850 hPa. During this period, a mixed layer was formed between 700 hPa and 500 hPa (not shown). From 0000 UTC to 1200 UTC 30 November, the temperature at 500 hPa and 700 hPa increased, while the temperature at 850 hPa continued to decrease. The mixing layer moved downward to form a capping inversion with the top at about 600

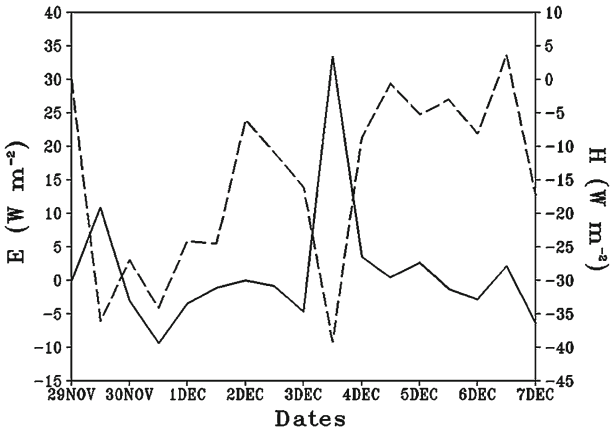

Fig. 11 Near-surface latent heat flux (*E*, *solid line*) and sensible heat flux (*H*, *dashed line*) at KSLC from 0000 UTC 29 November to 0000 UTC 7 December 2010

hPa and the base at about 760 hPa in the simulation. Meanwhile, a surface-based inversion formed near the ground.

Figure 10a shows that the temperature at 850 hPa started to increase at 0000 UTC 1 December. After that, the temperature at all three levels (500 hPa, 700 hPa and 850 hPa) increased gradually until 1200 UTC 3 December. The temperature increase at the lower level can be attributed to the heating by warm-air advection from the south of Salt Lake City. Then, the temperature decreased very slightly until 0000 UTC 6 December. From 0000 UTC to 1200 UTC 6 December, a strong upward motion brought air from lower to higher levels and caused temperature increases at all three pressure levels. When a cold trough passed over Salt Lake City, temperature at all three pressure levels decreased rapidly. As a consequence, the inversion weakened significantly.

Overall, as mentioned above, the life cycle of this persistent inversion depended on a change in the temperature structure. In the formation phase, the air was warmed aloft and cooled at lower levels with an intensification of the cold pool. From 0000 UTC 1 December to 0000 UTC 6 December, the temperature of the inversion layer first increased and then decreased. From 0000 UTC 6 December to 0000 UTC 7 December, the temperature of the whole layer first increased slightly, then decreased rapidly, resulting in a notable weakening of the persistent inversion. *It should be concluded that "warming" aloft and "cooling" at lower levels are necessary conditions for the formation of a persistent inversion. In addition, the "cooling" aloft is important for the weakening of the inversion.*

4.4.2 Latent and Upward Sensible Heat Fluxes at the Surface

The role of surface heating conditions in the evolution of the persistent inversion is also examined. Figure 11 presents simulated latent and upward sensible heat fluxes at the surface at the KSLC station from 0000 UTC 29 November to 0000 UTC 7 December. On 29 November, the sensible heat flux decreased rapidly due to snowfall during the day, corresponding to the onset of the inversion. Then, sensible heat fluxes increased during the persistent inversion but decreased rapidly on 3 and 7 December. Latent heat flux shows only moderate change during the whole period of the inversion except for a rapid change on 3 December due to a cold front passage. Both sensible heat flux and latent heat flux increased from 0000 UTC 6

and decreased from 1200 UTC 6 to 0000 UTC 7 December, corresponding to the extreme weakening of the inversion.

During the persistent inversion, the surface was covered with snow before 6 December. The effect of snow cover has been stated in Billings et al. (2006) and Jin and Miller (2007). Snow cover causes an increase in the surface albedo and cooling near the surface. Around 0000 UTC 7 December, the snow melted and the inversion was significantly weakened. Therefore, surface snow cover may provide one favourable condition for the formation and continuation of persistent inversions.

5 Sensitivity of the Numerical Simulation to WRF Model Vertical Resolution

It is commonly believed that high resolution numerical simulations can better resolve small-scale processes in the boundary layer. To examine the impact of model vertical resolution on the numerical simulation of near-surface atmospheric conditions, an additional set of early experiments is compared with the current simulation in order to examine the sensitivity of the model simulation to vertical resolution. In the early experiments, all other configurations, including model domains, horizontal resolution, and physics options are the same as in the current (control) simulation (as described in Sect. 3), except that 36 vertical levels (instead of 60 levels) are used. Note that the decrease in vertical levels from 60 to 36 is more obvious below 6 km of height, especially in the lowest 2 km.

Figure 12a compares the time series of temperature and wind profiles and the inversion top from the two simulations. Only slight differences in boundary-layer temperature and wind fields are found in the two simulations, although the simulation with 60 vertical levels performs slightly better when compared with soundings (Fig. 4). The simulation with 60 vertical levels also produces a better simulation of the inversion top, especially for the period between 30 November and 3 December.

Errors in the near-surface air temperature are also compared. The mean absolute error (*MAE*) of simulated 2-m temperature against the Mesonet observations is calculated, with *MAE* calculated from

$$MAE = \frac{1}{n}\sum_{i=1}^{n} |F_i - O_i| \tag{1}$$

where i denotes the ith observation, O_i represents the observed temperature at the ith location, F_i denotes the simulated temperature interpolated to the ith observation location, and n is the total number of stations. *MAE* is calculated over these stations in Salt Lake and Utah Valley (as shown in Fig. 7), and Fig. 12b compares *MAE* of the 2-m temperature from two simulations. Overall, improvement in surface forecasts is not ensured by increased vertical resolution. This result may imply that model errors associated with the coupling between the surface and near-surface atmosphere could play a significant role in predicting near-surface variables (as discussed in Hacker and Angevine 2012 and Cheng and Steenburgh 2005).

6 Summary and Conclusions

Salt Lake City, Utah, experienced a persistent inversion in the early winter of 2010. In this study, the WRF numerical model is used to simulate the life cycle of the event. Results indicate that the numerical simulation successfully reproduced the persistent inversion event. Except

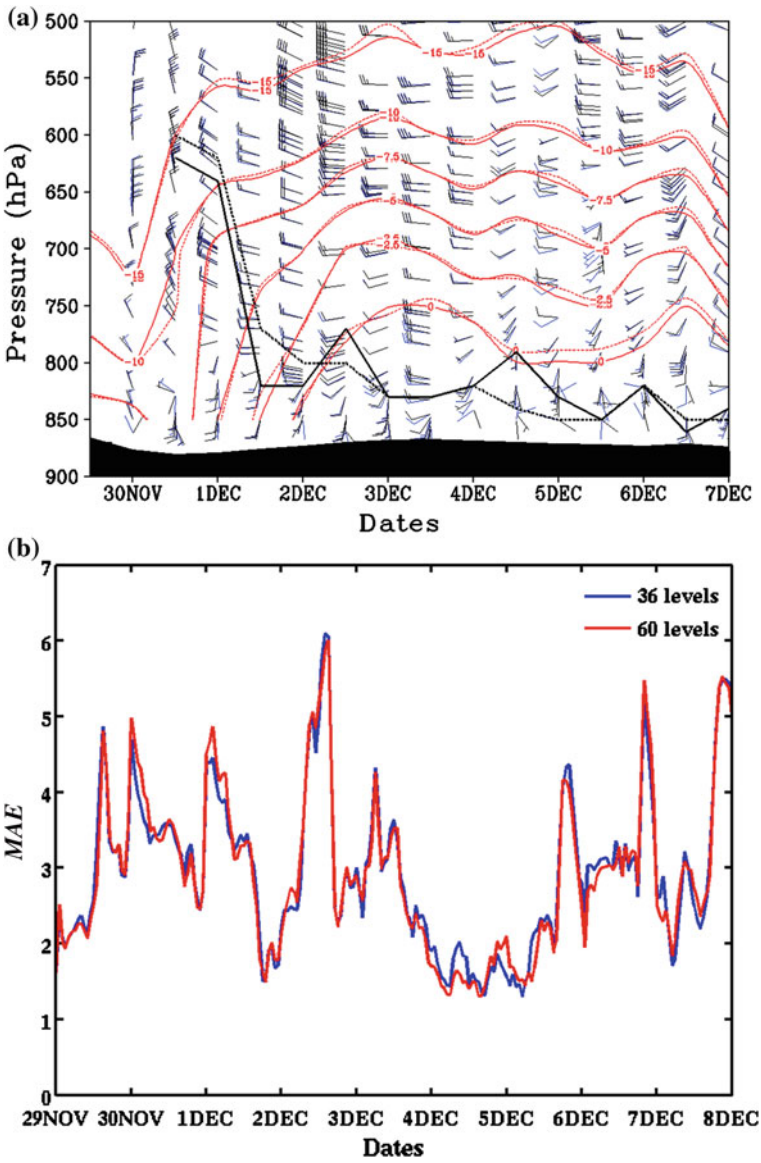

Fig. 12 **a** Same as Fig. 4, except for the solid (*dashed*) lines and black (*blue*) wind barbs are from the simulation with 36 (60) model vertical levels. **b** Comparison of the mean absolute error (*MAE*) of simulated 2-m temperature over Salt Lake and Utah valleys from two numerical simulations. The *blue curve* denotes the *MAE* from the simulation with 36 model vertical levels and the *red curve* shows the *MAE* from the simulation with 60 model vertical levels. Days are shown at 0000 UTC

for some discrepancies near the surface, the simulation results agree well with the soundings. Due to simulation error in the near-surface atmosphere conditions, the inversion top from the simulation is lower than that from the soundings during most of the persistent inversion period. However, the trend of the time variations of the inversion top from the simulation is consistent with that from the soundings. Although the WRF model has problems identifying

the type of inversion, the variation of inversion strength between the simulation and the observations is consistent most of the time. An inverse relationship is found between depth and strength from the soundings and the simulation.

Given the confidence gained from the accurate WRF simulation of the atmospheric conditions above the near-surface layer, we examine the large-scale processes, local circulation, and physical variables that contribute to the formation and persistence of inversions. It is found that:

- During the formation phase, a high-pressure ridge at 500 hPa supplied warm air aloft. At the surface, a cold air pool formed due to radiation effects, and meanwhile, cold air flowed into Salt Lake City from mountain slopes to the east. A mixed layer first formed between 700 hPa and 500 hPa around 0000 UTC 30 November, and then a capping inversion formed with the inversion top at about 600 hPa around 1200 UTC 30 November. With further surface cooling, a surface-based inversion formed. Around 0000 UTC 1 December, the capping inversion aloft moved downward to merge with the surface-based inversion and formed a capping inversion near the surface.
- During the continuation phase, a high-pressure ridge remained at 500 hPa, which ensured a supply of warm air aloft. During the period of 0000 UTC 1 December to 0000 UTC 3 December, there was almost no vertical motion, which ensured the inverted temperature structure. Relatively warm air from the south of Salt Lake Valley weakened the cold pool over Salt Lake City. The temperature of the whole layer increased; however, the inverted temperature structure was maintained. Around 1200 UTC 3 December, a cold front passed over Salt Lake City, resulting in increasing wind speed aloft with apparent downward motion, and the inversion top descended. From 0000 UTC 4 December to 1200 UTC 6 December, the horizontal advection and vertical motion were very weak, and coupled with cooling at the surface the strength of the inversion was enhanced.
- Around 1200 UTC 6 December, downward motion aloft occurred with upward motion at lower levels, resulting in the descent of the inversion top. Then, by 0000 UTC 7 December, a trough at 500 hPa passed over Salt Lake City with cold-air advection. Meanwhile, a low-pressure system was dominant in the lower atmosphere, resulting in a greatly weakened inversion.

During this episode, there was a relation between the upward sensible heat flux near the surface and the height of the inversion top. When the sensible heat flux decreased rapidly on 3 and 7 December, the height of the inversion top also decreased. In addition, latent and sensible heat fluxes had a similar variation trend in the formation and dissipation phases, but an opposite trend at other times. It should be noted that the simulation experiment performed in this study is at mesoscale resolutions (12-km, 4-km, and 1.33-km grid spacings). Simulation at these resolutions could have limitations in describing inversions near the surface in detail, resulting in defects in simulating the type of inversion. The increase of model vertical resolution only slightly improves the numerical simulation of the inversion, while the improvement in surface forecasts is not ensured. Model errors associated with the coupling between the surface and near-surface atmosphere could play a significant role in predicting near-surface variables. Future work will be conducted to study the detailed structure of inversions using a small-scale model, such as large-eddy simulation. The WRF model errors in the near-surface atmosphere, similar to those addressed in Bravo et al. (2008), will also be further evaluated.

Acknowledgments The authors would like to acknowledge the WRF model working group for their effort in developing a mesoscale community model system. The first author is supported by a Chinese overseas scholarship sponsored by the State Department of Education of China. The second author (ZP) is supported by the Office of Naval Research Award # N00014-11-1-0709. The computer time granted by the Centre for

High Performing Computing (CHPC) at the University of Utah is gratefully acknowledged. Comments from two anonymous reviewers were very helpful in improving the manuscript.

References

Billings BJ, Grubisic V, Borys RD (2006) Maintenance of a mountain valley cold pool: a numerical study. Mon Weather Rev 134:2266–2278

Bravo M, Mira T, Soler MR, Cuxart J (2008) Intercomparison and evaluation of MM5 and meso -NH mesoscale models in the stable boundary layer. Boundary-Layer Meteorol 128:77–101

Chen F, Dudhia J (2001) Coupling an advanced land-surface/ hydrology model with the Penn State/ NCAR MM5 modeling system. Part I: model description and implementation. Mon Weather Rev 129:569–585

Cheng WYY, Steenburgh WJ (2005) Evaluation of surface sensible weather forecasts by the WRF and the Eta models over the Western United States. Weather Forecast 20:812–821

Colette A, Chow FK, Street RL (2003) A numerical study of inversion-layer breakup and the effects of topographic shading in idealized valleys. J Appl Meteorol 42:1255–1272

Dudhia J (1989) Numerical study of convection observed during the winter monsoon experiment using a mesoscale two-dimensional model. J Atmos Sci 46:3077–3107

Gillies RR, Wang S-Y, Booth MR (2010a) Atmospheric scale interaction on wintertime intermountain west low-level inversions. Weather Forecast 25:1196–1210

Gillies RR, Wang S-Y, Yoon J-H, Weaver S (2010b) CFS prediction of winter persistent inversions in the intermountain region. Weather Forecast 25:1211–1218

Hacker JP, Angevine WM (2012) Ensemble data assimilation to characterize surface-layer errors in numerical weather prediction models. Mon Weather Rev (in press)

Holzworth GC (1962) A study of air pollution potential for the western United States. J Appl Meteorol 1:366–382

Holzworth GC (1967) Mixing depths, wind speeds and air pollution potential for selected locations in the United States. J Appl Meteorol 6:1039–1044

Hong S-Y, Dudhia J, Chen S-H (2004) A revised approach to ice microphysical processes for the bulk parameterization of clouds and precipitation. Mon Weather Rev 132:103–120

Horel J, Splitt M, Dunn L, Pechmann J, White B, Ciliberti C, Lazarus S, Slemmer J, Zaff D (2002) Mesowest: cooperative mesonets in the western United States. Bull Am Meteorol Soc 83:211–226

Janjic ZI (2002) Nonsingular implementation of the Mellor–Yamada level 2.5 scheme in the NCEP Meso model. NCEP Office Note No. 437, 61 pp

Jin J, Miller NL (2007) Analysis of the impact of snow on daily weather variability in mountainous regions. J Hydrometeorol 8:245–258

Kain JS, Fritsch JM (1990) A one-dimensional entraining/ detraining plume model and its application in convective parameterization. J Atmos Sci 47:2784–2802

Liu Y, Key JR (2003) Detection and analysis of clear-sky, low-level atmospheric temperature inversions with MODIS. J Atoms Oceanic Technol 20:1727–1737

Mlawer EJ, Taubman SJ, Brown PD, Iacono MJ, Clough SA (1997) Radiative transfer for inhomogeneous atmospheres: RRTM, a validated correlated-k model for the longwave. J Geophys Res 102:16663–16682

Müller H, Whiteman CD (1987) Breakup of a nocturnal temperature inversion in the Dischma Valley during DISKUS. J Appl Meteorol 27:188–194

Reddy PJ, Barbarick DE, Osterburg RD (1995) Development of a statistical model for forecasting episodes of visibility degradation in the Denver metropolitan area. J Appl Meteorol 34:616–625

Reeves HD, Stensrud DJ (2009) Synoptic-scale flow and valley cold pool evolution in the western United States. Weather Forecast 24:1625–1643

Skamarock WC, Klemp JB, Dudhia J, Gill DO, Barker DM, Duda MG, Huang X, Wang W, Powers JG (2008) A description of the advanced research WRF version 3. NCAR Tech. Note, NCAR/TN-475+STR, 113 pp

Wendisch M, Mertes S (1995) Vertical profiles of aerosol and radiation and the influence of temperature measurements and radiative transfer calculations. J Appl Meteorol 35:1703–1715

Whiteman CD, Pospichal B (2004) Inversion breakup in small Rocky Mountain and Alpine basins. J Appl Meteorol 43:1069–1082

Whiteman CD, Bian X, Zhong S (1999) Wintertime evolution of the temperature inversion in the Colorado Plateau Basin. J Appl Meteorol 38:1130–1117

Wolyn PG, McKee TB (1989) Deep stable layers in the intermountain western United States. Mon Weather Rev 117:461–472

Zoumakis NM, Efstathiou GA (2006a) Parameterization of inversion breakup in idealized valleys. Part I: the adjustable model parameters. J Appl Meteorol 45:600–608
Zoumakis NM, Efstathiou GA (2006b) Parameterization of inversion breakup in idealized valleys. Part II: thermodynamic model. J Appl Meteorol 45:609–623